



# Efficiency Enhancement of Thermophotovoltaic Cells With Different Design Configurations Using Existing Photon Recycling Technologies

Muhammad Usman<sup>1\*</sup>, Ali H. Kazim<sup>1\*</sup>, Aqsa Shabbir<sup>2\*</sup>, Muhammad Salman Abbasi<sup>1</sup> and Jawad Sarwar<sup>1</sup>

<sup>1</sup>Department of Mechanical Engineering, University of Engineering and Technology Lahore, Lahore, Pakistan, <sup>2</sup>Department of Electrical Engineering, Lahore College for Women University, Lahore, Pakistan

## OPEN ACCESS

### Edited by:

Yanwei Hu,  
Harbin Institute of Technology, China

### Reviewed by:

Meijie Chen,  
Central South University, China  
Haoran Li,  
Northeast Electric Power University,  
China

### \*Correspondence:

Muhammad Usman  
usmanme132@gmail.com  
Ali H. Kazim  
ali.h.kazim@uet.edu.pk  
Aqsa Shabbir  
Aqsa\_shabbir@outlook.com

### Specialty section:

This article was submitted to  
Solar Energy,  
a section of the journal  
Frontiers in Energy Research

**Received:** 11 April 2022

**Accepted:** 23 May 2022

**Published:** 25 July 2022

### Citation:

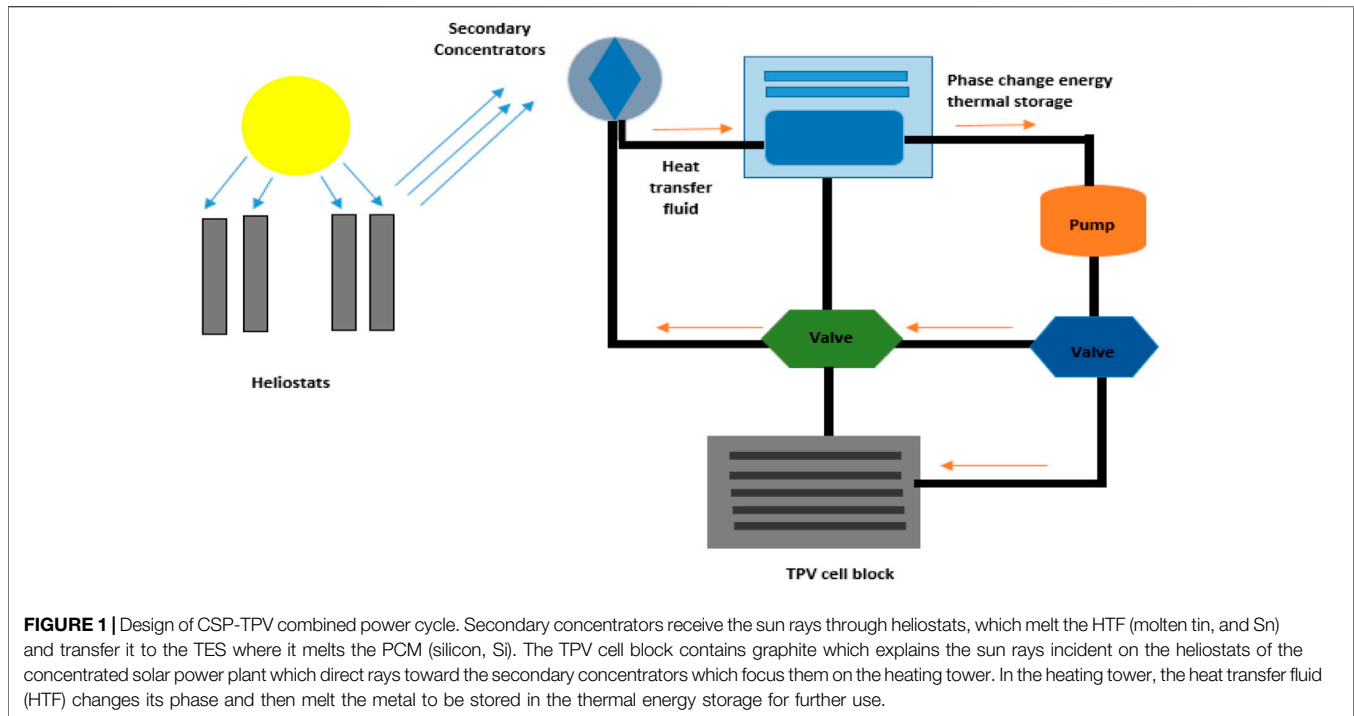
Usman M, Kazim AH, Shabbir A,  
Abbasi MS and Sarwar J (2022)  
Efficiency Enhancement of  
Thermophotovoltaic Cells With  
Different Design Configurations Using  
Existing Photon  
Recycling Technologies.  
Front. Energy Res. 10:917419.  
doi: 10.3389/fenrg.2022.917419

This work deals with different design configurations using existing photon recycling technologies such as front spectral filters and back surface reflectors (BSRs) to improve the efficiency of the thermophotovoltaic (TPV) cells. On the TPV cell surface, some photons absorb, but some quantity of them is lost due to the interference on the surface. On the other hand, BSR mounted on the backside of the cell reflects all photons which were not absorbed by TPV back to the front side of the cell and the emitter, which leads to the elevated temperature of the cell and more interference on the cell surface. This work aimed to design a configuration of the TPV system model using hybrid photon recycling technologies and to investigate the efficiencies of different TPV cells with numerous factors such as emitter temperature and reflectivity of the spectral filter. The design parameters and configuration of front filters with BSRs are studied under 2500 K temperature of the emitter. It is found that an InGaAs cell with reasonable bandgap energy of 0.72 eV, is the most favorable cell material as its bandgap wavelength (1.68  $\mu\text{m}$ ) is closely matched to the peak wavelength (1.65  $\mu\text{m}$ ) of the emissions spectra. The results show that the incorporation of magnesium oxide (MgO) spectral filter along with the BSR ( $R = 1$ ) and the emitter temperature of 2200 K efficiency as high as 35% can be attained. This makes MgO a viable choice in TPV cell system under concentrated solar power plant.

**Keywords:** thermophotovoltaics, photon recycling, thermophotovoltaic, design configuration, spectral filter, back surface reflectors

## 1 INTRODUCTION

The global energy crisis has increased due to the depletion of natural resources to meet the energy demands of the planet (Coyle and Simmons, 2014). Many countries use fossil fuels such as coal and natural gas, while some others use water and nuclear resources to generate electricity (Cherp et al., 2017; Onifade et al., 2021). Over the centuries, fossil fuels have been used for energy as they are an economical resource to rely on, for energy production. But they come up with the global warming problem which further leads to the problem of sea-level rise, fires, storms, and massive floods. Due to this, there is an increased interest in deploying renewable energy resources to meet the energy

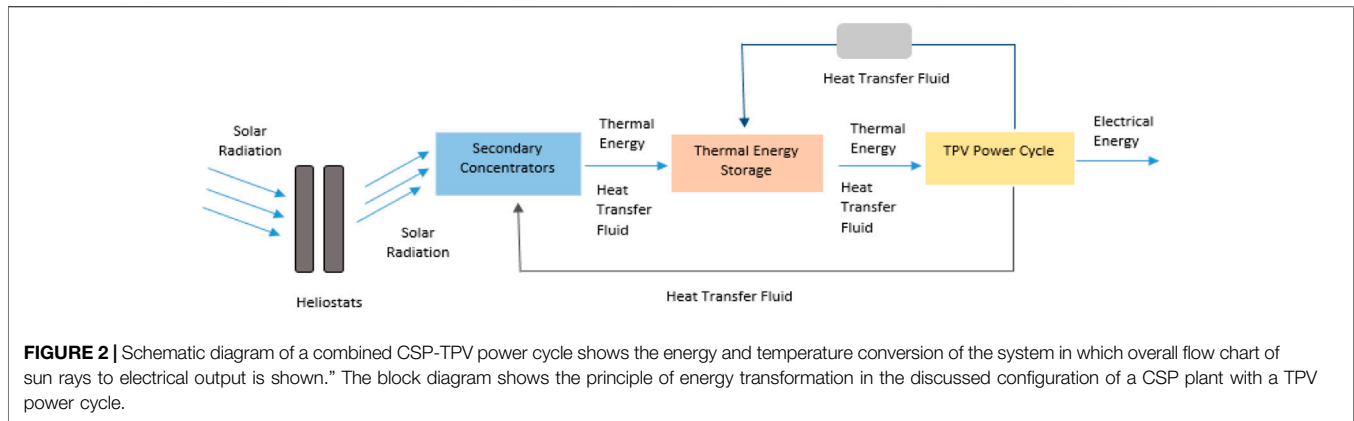


demand of the planet instead of relying solely on limited natural resources such as fossils (Romero et al., 2012; Li et al., 2014; Güneş, 2019; Hansen et al., 2019). The extreme consumption of these resources is responsible for environmental degradation (Hank et al., 2020). The solution to these problems lies in the fact that renewable energy resources should be used instead of non-renewables for power generation (Hansen et al., 2019). As reported, by 2050, two out of three global energy demands will be met by renewable resources (Goorha and Denmark, 2010).

Wind and solar renewable energy resources are examples of renewable energy resources, but they are not dependable as they depend on weather conditions (Barber, 2018; Jung et al., 2018; Warren et al., 2018; Cendula et al., 2019). However, increased research in the field of renewable energy resources can help overcome this problem (Kazim et al., 2020). Concentrated solar power (CSP) uses focused Sun rays to generate electrical power and is widely used nowadays. Concentrated solar power also faces a lot of the irradiation at their surface due to which efficiency is decreased as irradiation is increased (Chen et al., 2016a). We cannot extract photons from the CSP as they cannot be stored for a longer period (Kazim et al., 2020). Thermophotovoltaics (TPVs) can be used in addition to the CSP, as it converts solar radiation to an intermediate form of energy (Boriskina et al., 2015). TPV is composed of a system that converts the electromagnetic radiation source from a heated body to the electrical power through photovoltaics (Datas and Vaillon, 2021). Renewable energy resources like thermophotovoltaics (TPVs) have emerged over the last decade to replace fossil fuels. Although there are many modern fossil plants that use combined cycle power plants to decrease the heat waste. Current CSP combined cycles have an efficiency of about 35–40% (Henry et al., 2014). TPV conversion of this heat waste into electricity is a

promising technology. A TPV technology takes the heat from the heat source of the CSP, and this heat energy is further converted into electrical energy. TPV paired with CSP also utilizes lesser area for equipment (Seyf et al., 2016). TPV has extremely high reliability, low noise, high gravimetric, and long operation time advantages. TPV cells use a variety of heat sources such as chemical, nuclear, solar, and waste heat, which heats up radiators commonly known as emitters whose temperatures go up to 1,300–2,000 K (Nelson, 2003).

A CSP-TPV combined power cycle is shown in **Figure 1** which explains the Sun ray incident on the heliostats of the concentrated solar power plant which direct rays toward the secondary concentrators which focus them on the heating tower. In the heating tower, the heat transfer fluid (HTF) changes its phase and then melts the metal to be stored in the thermal energy storage for further use. The electrical power output, efficiency, and incident radiations of a TPV module are calculated using MATLAB. Secondary sources receive the reflected Sun rays from heliostats. The heat transfer fluid (HTF) heats up via the secondary collectors and goes to the thermal energy storage (TES) where it cools down and gets pumped back to repeat the cycle (Kazim et al., 2020). The schematic diagram in **Figure 2** shows the energy and temperature conversion of the system in which overall flow chart of Sun rays to electrical output is shown.  $T$  and  $T_{melt}$  represent the temperature of the graphite emitter pipes and the temperature of the phase change material (PCM). The TES stores the thermal energy by melting the PCM via the heat of the HTF and maintains the temperature of the HTF that must enter the TPV cycle. Under high partial shading conditions (PSC), the HTF does not attain a temperature high enough to melt the PCM, now when HTF passes from the TES the PCM releases energy and heats up the HTF. Valves are fitted in the



system to maintain the unidirectional flow of the HTF as they prevent the HTF from flowing back to the TES and collectors from the TPV power cycle (Kazim et al., 2020). Many other solar thermal conversion and thermal energy storage of phase change composites materials are used such as CuO/paraffin (Chen et al., 2019). The TPV power cycle consists of a hexagonal cell cavity that is surrounded by water and a filter, TPV cells, and a BSR enclosed in a graphite pipe. Graphite has a high emissivity value ( $>0.90$ ) (Midilli et al., 2006) which makes them a good choice for use in these pipes. Most of the research that has been conducted utilizes the flat vertical plate TPV cell used in between emitter pipes. The hexagonal cavity used as its view factor is the same as that of the circular pipes (Yuksel et al., 2015). The performance of the TPV cells varies with the effect of temperature and radiations wavelengths that fall onto its surface, which is why most of the TPV cell arrays are equipped with spectral controls such as back surface reflectors (BSRs) and spectral filters as most of the emissions from the back body are below the bandgap (Rahmlow et al., 2007). The cell also receives the emission spectrum from the emitter which leads to the feverish temperature of the cell. Filters are used to improve the efficiency by removing any below-bandgap photons from the emission spectra of the emitter. The spectral filters are placed between the emitter and the TPV cell as they filter the photons that are below the bandgap of the TPV cell back to the emitter and let pass the higher bandgap photons as is (Rahmlow et al., 2004; Rahmlow et al., 2007; Chirumamilla et al., 2019). The photons with energy lower than the bandgap of the TPV cell cannot play part in transitions so they are filtered beforehand to reduce any interference at the surface of the cell and to keep the cell temperature lower (Rahmlow et al., 2007). On a TPV cell's surface, photons are absorbed, but some quantity of them is lost due to the interference on the surface. BSR is placed behind the TPV cells (Kazim et al., 2020). BSR mounted on the backside of the cell reflects the unabsorbed photons that are passed unabsorbed from the cell back to the active area of the TPV cell for the reabsorption which helps in increased efficiencies (Datas and Vaillon, 2021). BSR also reflects the below-bandgap photons back to the emitter and the emitter temperature is increased which improves the efficiency of the system (Wang et al., 2003). The specifications of the single-junction InGaAs

(McClelland and Mankin, 2018) cells that are used in a TPV array are such that the top contact layer of InGaAs is  $0.025 \mu\text{m}$  thick, which is followed by an emitter layer that is  $0.1 \mu\text{m}$  thick. The other three layers are as follows, the InGaAs base layer, InP buffer layer, and the InP substrate layer which are  $2.5$ ,  $0.3$ , and  $625 \mu\text{m}$  thick, respectively (Kazim et al., 2020).

The thermophotovoltaic systems are not much efficient without any spectral control, and they have only a fraction of energy converted to electricity which is 16–18% approximately (Ferrari et al., 2014). There is a potential in improving the conversion efficiencies of TPV systems by optimizing the TPV device's design, design of the cavity, and other fabrication configurations which include the use of multilayer TPV cells, BSRs, and spectral filters (Phan et al., 2009). Wavelength-selective emitters achieve better TPV performance than Ti and Ni filters. The nanoparticle material-based emitters show suitable results with low bandgap PV cells (Chen et al., 2021). It has also been observed with high refractive index materials such as antimony selenide, antimony sulfide, and gallium telluride as a spectral filter in TPV which possibly achieve 20% efficiency at a temperature of  $363.15 \text{ K}$  for a  $0.6 \text{ eV}$  band of cell (Rahmlow et al., 2007). The TPV cell of the GaSb cell using the waste heat recovery with the spectral technology of the front filter at the operating temperature of  $1,300\text{--}3,100 \text{ K}$  was found to be 21.57% energy conversion efficiency (Utlu, 2020). Wernsman et al. (2004) calculated the efficiency with the use of the back surface reflector which is 23.6%. Another configuration is used in the back surface reflector which is known as the hybrid back surface reflector GaInAsSb TPV device. In this configuration, the GaInAsSb-based TPV cell is constructed and a surface reflector is mounted on the backside which has the potential of recirculating the infrared photons which further helps to improve the efficiency (Huang et al., 2004). For InGaAs cell of  $0.74 \text{ eV}$ , the recent study attained more than 15% TPV efficiency which becomes more than 30% with reflectivity of 100% which made TPV favorable for concentrated solar power plants at a temperature of emitter more than  $2,000 \text{ K}$  (Kazim et al., 2020). The aforementioned techniques are commonly used in TPV to increase efficiency, but up to an extent. There must be further improvements needed to work on TPV as it has significant room for improvements, unlike other solid-state heat

engines which are currently operating at their thermodynamic limits as compared to other heat engines.

This study is based on efficiency enhancement with the combination of spectral controls, that is, the use of spectral filters along with existing photon recycling technologies such as BSR to improve the efficiency of the TPV system beyond 30%. Before this only front filters or back surface reflectors were used to recycle the photons, but in this study, the front filter is used to stop the low bandgap photons which create the interference on the surface of the TPV cell. This technique reduces the interference on the TPV cell which also decreases the temperature reducing the waste heat which is lost in cooling the cell. Furthermore, the use of spectral filters will maintain the temperature of the cell, lesser energy will be utilized for cooling the cells and they also suppress the amount of interference on the surface of the cell by removing lower bandgap photons from the emission spectra and hence achieve better efficiencies than only BSRs (Isobe et al., 2020; Sergeev and Waits, 2020). It also includes the investigation of factors such as EQE, emitter temperature, back surface reflectors, and spectral filters on the efficiency of the TPV cell. **Section 2** includes the materials that can be used for TPV cells, losses in a TPV system, and the use of different spectral control techniques. **Section 3** presents the methodology followed throughout the study, which is followed by **Section 4** which outlines the results and accompanying discussion. **Section 5** concludes the study.

## 2 THERMOPHOTOVOLTAIC SYSTEMS

### 2.1 TPV Cell

The photovoltaic cells that are used in a TPV system use single-junction cells, but a multijunction cell can also be used (Datas and Cells, 2015). Many cells are compared in this study, which includes silicon (Si), germanium (Ge), silicon-germanium (SiGe), gallium antimonide (GaSb), indium gallium arsenide (InGaAs), indium gallium arsenide antimonide (InGaAsSb), gallium arsenide (GaAs), cadmium telluride (CdTe) (Midilli et al., 2006). Silicon-based TPV models have been used for many years, as Si has a bandgap of 1.12 eV at 300 K. Si has a single-crystal structure and belongs to the IV group. Ge has the lower bandgap energy of 0.66 eV and their conversion efficiency is 6.7%, these cells show poor performances and are used in multijunction solar converters. BSRs are usually feasible for the Ge cells as their major challenge is the high voltage factor (Kazim et al., 2020). SiGe cells can have an altered bandgap in between the range of 0.66 and 1.12 eV, and this bandgap can be tuned with the change in the composition of the cell (Pethuraja et al., 2012). InGaAs ( $\text{In}_x\text{Ga}_{1-x}\text{As}$ ) cells can have a bandgap ranging from 0 to 1 by changing the stoichiometry (i.e., the value of  $x$ ) of the cells (Cabrerá et al., 2018). GaSb cells have a conversion efficiency of 3% which can be improved to 18%. These cells have a bandgap of 0.72 eV and are the best choice for TPV generators. InGaAsSb has the tunable bandgaps and the lattice constants (Midilli et al., 2006) GaAs and CdTe have high absorptivity which allows us to use a layer of only a few microns (Kazim et al., 2020).

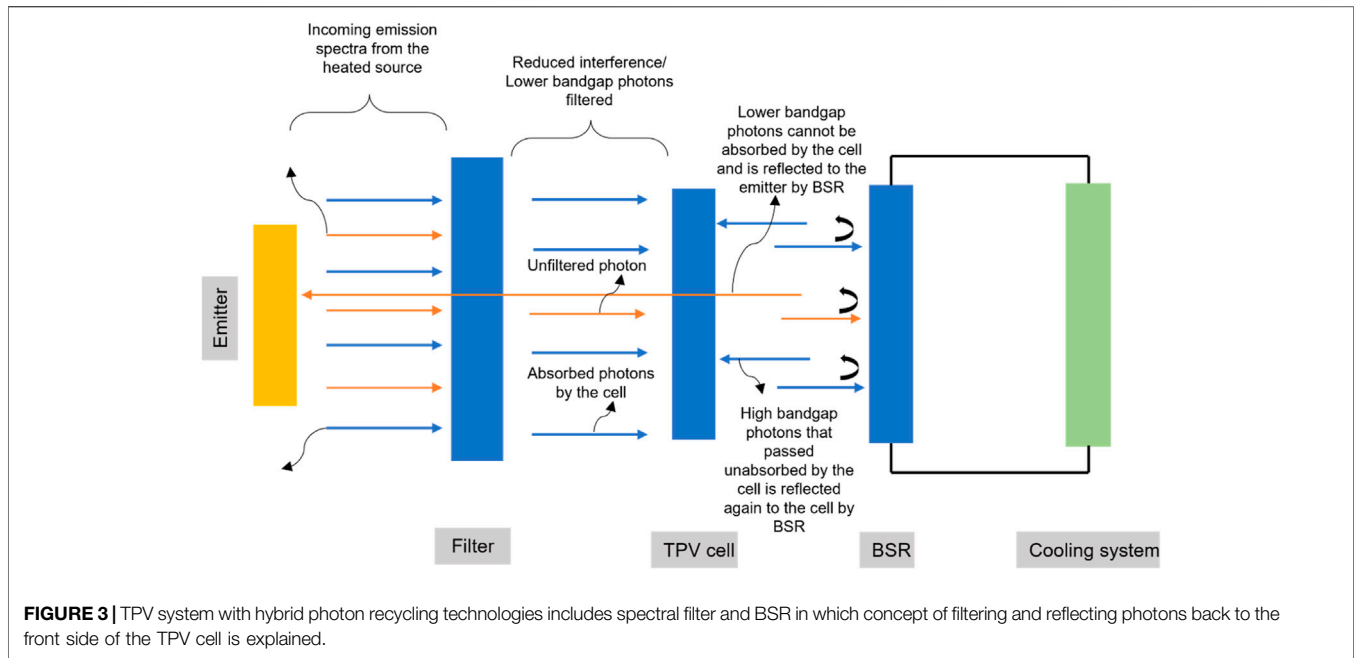
### 2.2 Optical Losses in the TPV System

The efficiency of TPV systems is reduced due to many practical losses, which can be enhanced by improving the components of the system (Seyf et al., 2016). These losses include the thermalization losses (Heidarzadeh et al., 2020) which are caused when the energy in the emission spectra is much higher than the energy of the bandgap and this also results in the heating of the cell. Non-absorption losses occur when the opposite happens, and the bandgap energy is higher than the energy in the emission spectra (Boulkhrachef, 2019). In other words, the emission spectra from the emitter consist of low bandgap photons that cannot take part in transitions and hence generate electrical power (Rahmlow et al., 2007).

These lower bandgap photons also create interference when they collide with the high bandgap photons at the surface of the cell. Due to this interference, much of the useful photon flux passes through the cell and goes without absorption, and energy is lost (Rahmlow et al., 2007). On the other hand, if the cell absorbs these lower bandgap photons they also result in additional heating of the cell and more energy is lost in the cooling of the TPV cell (Rahmlow et al., 2007). The reflective losses occur because photons get reflected from the top layer and due to the large emitter–cell distance they are not reabsorbed, and the transmission losses occur because of the cell's layer thickness (Nicholas and Tuley, 2012; Bernardi et al., 2015). Other losses also include radiative and non-radiative recombination losses which result in the recombination of the generated electron-hole pair and a photon, and a phonon are released, respectively, based on the properties of the cell's material (Yu and Zunger, 2012).

### 2.3 Photon Recycling

A TPV cell should be paired with photon recycling technologies to minimize the mentioned losses. Photon recycling refers to the methods in which only the photons that can be converted to the useful electrical power are allowed to reach the TPV cell and the non-convertible photons are suppressed and not able to reach the cell's surface (Rahmlow et al., 2007). This is also referred to as spectral control and there are different approaches to control the spectra. The cell should be placed close to the emitter to have the least edge effect and the view factor of nearly 1. The bandgap of a TPV cell should be closely matched to the blackbody radiation of the emitter and the peak wavelength of the spectrum so that a major part of the incoming photon flux is converted to electrical power (Rahmlow et al., 2007). The selective emitters emit the spectrum in a specific wavelength region when they are heated (Sakakibara et al., 2019). The selection of emitter material that allows such suppressive emissions is difficult and should be the cost-effective option. These emitters are composed of photonic crystals and rare earth metals (Sakr et al., 2014; Wang et al., 2014; Zhou et al., 2016a; Kim et al., 2018). Another method for spectral control is to add the filters between the heat source and the cell. The longer wavelength (lower bandgap) photons included in the emission spectra of the emitter, create interference at the cell's surface when they collide with the shorter wavelength (high bandgap) photons, and much of the useful photon flux passes unabsorbed from the cell (Rahmlow et al., 2007) and the temperature of the cell is also increased. Spectral filters do not



transmit the below-bandgap (long wavelength) photons, from the incoming spectrum, and reflect them back to the heated body (Erdoğan et al., 2010; Chirumamilla et al., 2019). This way the lower energy photons are filtered before reaching the surface of the TPV cell and only high bandgap photons that can play part in transitions reach the cell. There is reduced optical loss due to interference at the surface of the cell and the temperature of the cell is not increased. Hence, less energy is lost in cooling the cell (Rahmlow et al., 2004; Rahmlow et al., 2007; Chirumamilla et al., 2019). The BSR, placed behind the TPV cell, reflects back low and high bandgap photons, that went unfiltered and unabsorbed from the cell, back to the emitter and the front face of the TPV cell, respectively (Kazim et al., 2020; Datas and Vaillon, 2021), which further improves the efficiency of the TPV systems. **Figure 3** shows the schematic of the mentioned procedure and how the incorporation of both the spectral filters and BSRs in a TPV system enhances the number of useful spectra from the emitter. In **Figure 3**, emitters which are graphite rod are shown which emit the radiations and the front spectral filter of MgO which stops the low bandgap photons reaching on the TPV cell front side. The TPV cell is placed in between the front filter and back surface reflector, after the TPV cell back surface reflector is placed which reflects all the unabsorbed radiations back to the TPV front side. The back surface reflector is attached to the backside of the TPV cell which is also mounted with a cooling system which maintains the TPV cell temperature to 300 K.

### 3 METHODOLOGY

The TPV system including the photon recycling technologies is modeled using MATLAB. The configuration of the TPV system has been made with the basic spectral control technologies, that is , front filters and BSRs. The simulation was run by changing the

different cell types such as silicon, germanium, and other cells, varying emitter temperature, and reflectivity of the filters. Then, the efficiency of the TPV cells is calculated and the parameters that influence the improvement of the TPV device’s efficiency are concluded. **Figure 4** represents the mentioned procedure in the form of a flow chart which explains the TPV system is modeled using MATLAB which encounters the variables that stop the low bandgap photons from reaching the front surface of the TPV cell, and then BSR variables reflect the unabsorbed photons back to the front side of the TPV cell. In this manner, the efficiency of different cells by varying the emitter temperature and reflectivity of BSR is calculated.

#### 3.1 Cell Selection

The emissions from the graphite emitter are given by the Plank distribution function for the black bodies (Pfiester and Vandervelde, 2017) and the factor  $\epsilon$  includes all the defects in the emissions. So, the emissive power  $E$  in  $W/m^2$  within a certain wavelength  $\lambda$  band is given by **Eq. 1** (Yuan et al., 2015).

$$E(\lambda, T) = \int_{\lambda_1}^{\lambda_2} \frac{\epsilon \times C_1}{\lambda^5 \left[ e^{\left(\frac{C_2}{\lambda T}\right)} - 1 \right]} d\lambda \quad (1)$$

where  $C_1 = 3.742 \times 10^8 W/m^2\mu m^{-4}$ ,  $C_2 = 1.4388 \times 10^4 K\mu m$ , and  $T$  is the temperature of the emitter in kelvin.

Wein’s displacement law given by **Eq. 2** gives the value of the wavelength at which the emissive spectra is at its peak.

$$\lambda_p \times T = 2898\mu m.K \quad (2)$$

The aforementioned equation shows that there is an inverse relationship between the peak wavelength and the emitter temperature. The bandgap wavelength  $\lambda_g$  should be larger than the peak wavelength  $\lambda_p$ . Excessive thermalization losses

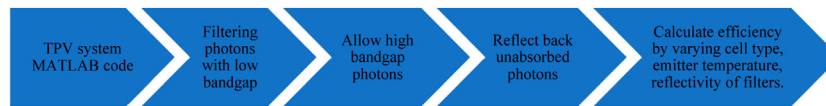


**FIGURE 4 |** Flow chart representing the followed methodology which represents the mentioned procedure in the form of a flow chart which explains the TPV system is modeled using MATLAB which encounter the variables that stops the low bandgap photons reaching the front surface of TPV cell then BSR variables reflects the unabsorbed photons back to the front side of the TPV cell.

occur if  $\lambda_g$  is very large than  $\lambda_p$ . However, bandgap wavelength  $\lambda_g$  can be found by the bandgap energy of the cell in eV given by Eq. 3 in the following equation (Anjani, 2021).

$$\lambda_g = \frac{hc}{E_g q} \tag{3}$$

where  $h$  is the Planck’s constant,  $c$  is the speed of light, and  $q$  is the charge of an electron in Coulombs. The photons above the bandgap region, which have a wavelength shorter than  $\lambda_g$ , are included in the useful spectrum of the TPV cell. The percentage of energy above the bandgap  $\eta_{E > E_g}$  (Bouزيد and Dehimi, 2012) is given by the proportion of these photons above the bandgap and is estimated as follows:

$$\eta_{E > E_g} = \frac{E_{(\lambda_{min} \rightarrow \lambda_g)}}{E_{b(0 \rightarrow \infty)}} \times 100\% \tag{4}$$

The total emitted power of the spectrum is calculated as follows, where  $\sigma$  is the Stefan–Boltzmann constant.

$$E_{b(0 \rightarrow \infty)} = \int_0^\infty \frac{\epsilon \times C_1}{\lambda^5 \left[ e^{\frac{C_2}{\lambda T}} - 1 \right]} d\lambda = \epsilon \sigma T^4 \tag{5}$$

### 3.2 Filter Selection

As stated, it is essential to place an optical filter between the emitter and the TPV cell to enhance the efficiency conversion of the overall system. The filter must have low absorptance and be highly transmissive, and it should be able to transmit the photons that have energy greater than the bandgap energy of the cell ( $E_p > E_g$ ) and hence lies in the useful range.

Similarly, it should have large reflectance for the photons that have energy lower than the bandgap energy of the cell ( $E_p < E_g$ ), as these photons cannot play part in transitions. The filter must have a wide spectral range and high melting points to sustain the incoming heat from the emitter. There are numerous filter technologies involving frequency selective surface (FSS), transparent conducting oxide (TCO), and all-dielectric filters (Bouزيد and Dehimi, 2012). FSS are periodic arrays made of conducting oxides deposited on a dielectric substrate. These are band-pass filters and they do not allow the photons above the bandgap energy of the cell (Hristov, 2016). TCOs are also commonly known as plasma filters and these are the doped semiconductors with large bandgaps (Köstlin, 1982; Coutts, 1999). All-dielectric filters, also known as interference filters, are composed of thin layers of materials having different

refractive indices (Coutts, 1999). Some filtering technologies also include the use of crystalline or polycrystalline materials for spectral control as listed in Table 1 (Machrafi, 2012).

Currently, no nanoparticles have the photostability, suitable wavelength transparency, and near-infrared emission specifically for the TPV cell of InGaAs (Khalid et al., 2019). Apart from these properties, the MgO spectral filter is stable under the temperature conditions of up to 2800 K. MgO contributes by filtering the photons up to 0.4  $\mu\text{m}$ . Contrary to this,  $\text{Y}_2\text{O}_3$  is another suitable choice due to its light composition and wide spectra in wavelength and high temperature resistivity (Zhou et al., 2016b; Lee, 2018).

### 3.3 BSR Selection

BSRs are placed in the TPV systems behind the cell. They act as spectral control as they reflect back the low bandgap photons back to the emitter and they also help in improving the efficiency of the cell as they increase the intensity of the high bandgap photons at the active layer of the cell for the second pass absorption, that lie in the range of the cell (Wang et al., 2003; Kazim et al., 2020; Datas and Vaillon, 2021). BSRs must have high thermal stability and strong adhesion (Charache et al., 1996). Highly reflective materials with less absorbance, including metals like gold (Au) and silver (Ag) can be used as BSR (Machrafi, 2012; Datas and Cells, 2015; Chen et al., 2016b; Seyf et al., 2016; Karalis and Joannopoulos, 2017).

### 3.4 Characterization of the TPV System

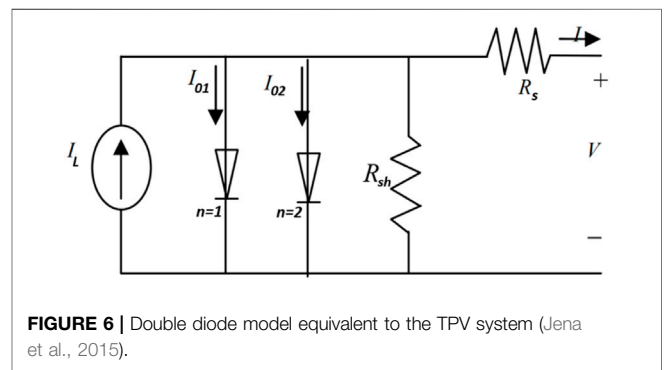
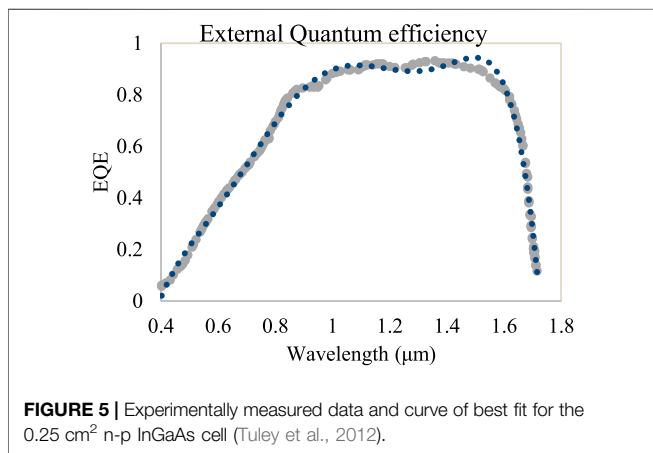
#### 3.4.1 External Quantum Efficiency

External quantum efficiency (EQE) tells the probability of photons that have been incident on the TPV cell absorbed by the cell and used in generating charge carriers (Ferrari et al., 2014) within the cell. The EQE of the photons with energy below the bandgap energy is zero. EQE is exclusively characteristic of the TPV cell device irrespective of the characteristics of the emitter (Kazim et al., 2020). Ideally, the EQE must be constant and equal to 1 but due to many losses that occur within the cell, radiative and non-radiative recombination losses are among those (Shockley and Queisser, 1961), the EQE shows an irregular behavior (Kazim et al., 2020).

The EQE data of the TPV cell can be determined experimentally or are also provided by the manufacturer of the cell. It is unique for all cells. Such an EQE plot for a 0.25  $\text{cm}^2$  n-p InGaAs cell has been drawn in Figure 5, using the experimental data given by Tuley et al. (2012) and the equation mentioned.

**TABLE 1** | Crystalline materials used as spectral filters along with their melting points.

Material	Chemical symbol	Melting point (°C)	Temperature for a vapor pressure of 1.33 E-2 Pa (°C)	Transparency range (-pm)
Boron phosphide	BP	1,125 decomp	N/A	0.5–N/A
Barium titanate	BaTiO <sub>3</sub>	1,625	N/A	N/A
Yttrium aluminum oxide	Y <sub>3</sub> Al <sub>5</sub> O <sub>12</sub>	1,930	N/A	0.2–5
Strontium titanate	SrTiO <sub>3</sub>	2,080	N/A	0.5–5
Spinel	MgAl <sub>2</sub> O <sub>4</sub>	2,135	N/A	0.2–5
Aluminum oxynitride	Al <sub>23</sub> O <sub>27</sub> N <sub>5</sub>	2,170	N/A	0.2–5
Diamond	C	~3,500	N/A	0.2–3
Zinc selenide	ZnSe	1520	660	0.5–19
Zinc sulphide (wurtzite)	ZnS	1,700	800	0.4–12.5
Silicon nitride	Si <sub>3</sub> N <sub>4</sub>	1,900	800	N/A
Gallium phosphide	GaP	1,457	920	0.5–N/A
Lanthanum fluoride	LaF <sub>3</sub>	1,493	900	0.1–10
Silicon carbide	SiC	2,830	1000	0.5–4
Magnesium oxide	MgO	2,825	1300	0.4–7
Titanium oxide	TiO <sub>2</sub>	1,560–1,843	1,300	0.4–4
Silicon	Si	1,414	1337	1.1–6.5
Sapphire	Al <sub>2</sub> O <sub>3</sub>	2,054	1,550	0.2–5
Boron nitride	BN	2,967	1,600	0.2–N/A
Aluminum nitride	AlN	3,000	1,750	N/A
Yttria	Y <sub>2</sub> O <sub>3</sub>	2,439	2,000	0.3–7



$$EQE(\lambda) = -55\lambda^8 + 441.46\lambda^7 - 0.0015\lambda^6 + 0.0029\lambda^5 - 0.0034\lambda^4 + 0.0025\lambda^3 - 0.0011\lambda^2 + 260.91\lambda - 26.89 \quad (6)$$

The average external quantum efficiency  $\overline{EQE}$  for the wavelength equal to or smaller than the bandgap wavelength is given as follows:

$$\overline{EQE} = \frac{1}{\lambda_g - \lambda_{min}} \left( \int_{\lambda_{min}}^{\lambda_g} EQE(\lambda).d\lambda \right) \quad (7)$$

where  $\lambda_{min}$  is the shortest wavelength for which the EQE has been recorded. The calculated  $\overline{EQE}$  for a 0.25 cm<sup>2</sup> n-p InGaAs cell is 0.7097.

### 3.4.2 Double Diode Model

The double diode model is equivalent to the TPV system design used here, and it represents the voltage–current behavior of the

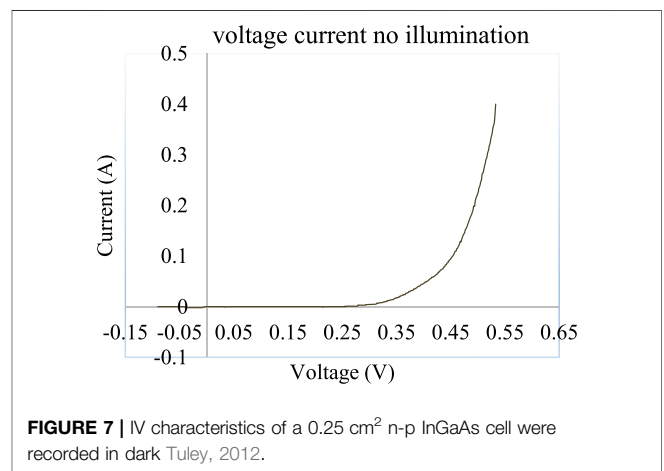


**TABLE 2** | Different PV cell materials are compared.

Materials	$E_g$ (eV)	$\lambda_g$ ( $\mu\text{m}$ )	$\lambda_g - \lambda_p$ ( $\mu\text{m}$ )
InGaAsSb	0.55	2.25	0.60
Ge	0.66	1.88	0.22
GaSb	0.72	1.72	0.07
InGaAs	0.74	1.68	0.02
CIS	1.00	1.24	-0.42
Si	1.12	1.11	-0.55
CdTe	1.50	0.83	-0.83
CGS	1.70	0.73	-0.93

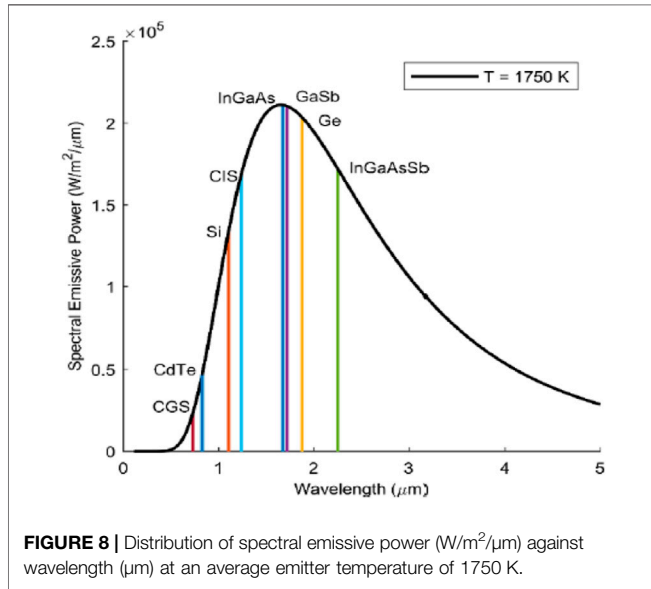


**FIGURE 8** | Distribution of spectral emissive power ( $\text{W}/\text{m}^2/\mu\text{m}$ ) against wavelength ( $\mu\text{m}$ ) at an average emitter temperature of 1750 K.

system. The second diode incorporates the recombination losses in the depletion region (Jena et al., 2015). The equation gives the current-voltage characteristics (Hejri et al., 2014) of the model and **Figure 6** represents the circuit diagram for the double diode model.

$$I = I_L - I_{01} \left( e^{\frac{q(V+IR_s)}{n_1 k T_c}} - 1 \right) - I_{02} \left( e^{\frac{q(V+IR_s)}{n_2 k T_c}} - 1 \right) - \frac{V + IR_s}{R_{sh}} \quad (8)$$

$I_L$  is the photocurrent in ampere,  $I_{01}$  and  $I_{02}$  are the anti-parallel saturation current of diodes one and two, respectively,  $n_1$  and  $n_2$  are the ideality factors of the diodes one and two taken as 1 (Riřland and Breitenstein, 2013) and 2 (Breitenstein et al., 2013), respectively.  $T_c$  is the temperature of the cell in kelvin,  $k$  is the Boltzmann constant while,  $R_s$  and  $R_{sh}$  are the series and shunt resistances, respectively. The shunt resistance must be very much greater than the series resistance in the circuit. Some assumptions are made to simplify **Eq. 8**, which include neglecting -1 from 2<sup>nd</sup> and third terms, also that  $R_{sh}$  is very large due to very high quality of cell fabrication and a large amount of photon injection. So, the simplified equation becomes as follows:

$$I = I_L - I_{01} \left( e^{\frac{q(V+IR_s)}{k T_c}} \right) - I_{02} \left( e^{\frac{q(V+IR_s)}{2k T_c}} \right) \quad (9)$$

### 3.4.3 The IV Characteristics

The photon flux  $\phi$  ( $\text{m}^{-2}\text{s}^{-1}$ ) (Norton et al., 2015) is the number of photons having energy greater than or equal to the bandgap energy emitted by the emitter per unit time and is given as follows:

$$\phi (\text{m}^{-2}\text{s}^{-1}) = \frac{E(\lambda_{min} \rightarrow \lambda_g)}{\left( \frac{1}{(\lambda_{min} + \lambda_g)} (10^{-6}) \right) \left( \int_{\lambda_{min} \times 10^{-6}}^{\lambda_g \times 10^{-6}} \frac{hc}{\lambda} d\lambda \right)} \quad (10)$$

The denominator in **Eq. 10** denotes the average energy of photons from the emitter, and wavelengths ranging from  $\lambda_{min}$  to  $\lambda_g$ .  $I_L$  is the photocurrent (Midilli et al., 2006) when the TPV device is illuminated and is calculated as follows:

$$I_L = \text{Area of module} \times q \times \phi \times \underline{EQE} \quad (11)$$

The dark saturation current  $I_{01}$  and  $I_{02}$  can be found by putting  $I_L = 0$ , so **Eq. 9** becomes

$$I = I_{01} \left( e^{\frac{q(V+IR_s)}{k T_c}} \right) + I_{02} \left( e^{\frac{q(V+IR_s)}{2k T_c}} \right) \quad (12)$$

The dark saturation currents are calculated by simultaneously solving **Eq. 12** using two sets of measured currents at the voltage values of 0.35 V and 0.41 V, under dark conditions.

**Figure 7** shows the IV characteristics of a 0.25  $\text{cm}^2$  n-p InGaAs cell.  $I_{01}$  and  $I_{02}$  are found experimentally by putting  $R_s = 0.25 \text{ m}\Omega\text{cm}^2$  and a set of other experimental data recorded in the dark (Tuley et al., 2012). The potential difference across the external circuit when the net current through the external circuit is zero is called as the open-circuit voltage  $V_{OC}$ . It can be found by modifying **Eq. 9** as follows (Meyer, 2017):

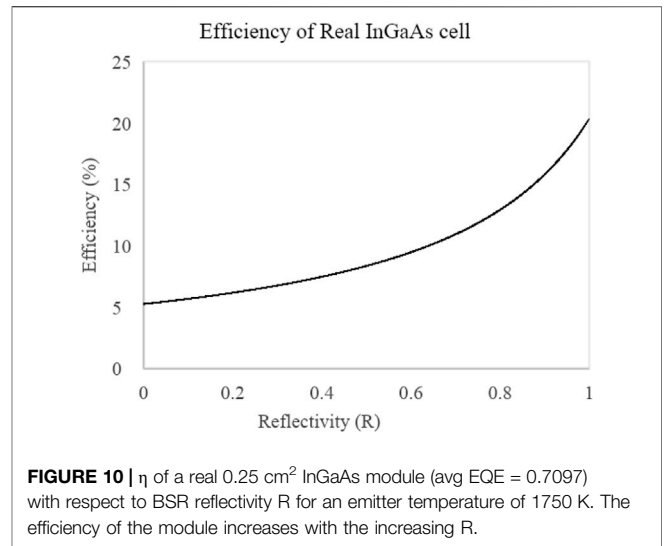
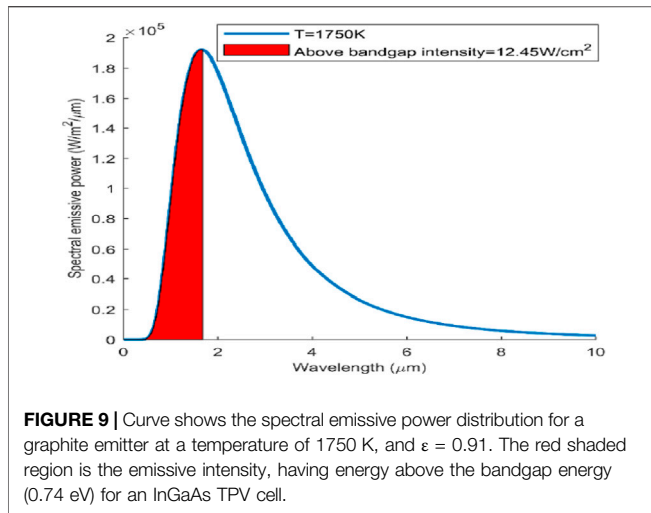
$$I_L = I_{01} \left( e^{\frac{q(V_{OC})}{k T_c}} \right) - I_{02} \left( e^{\frac{q(V_{OC})}{2k T_c}} \right) \quad (13)$$

Fill factor  $\eta_{FF}$  is the ratio of the product of the  $V_m$  and  $I_m$  to the product of  $V_{OC}$  and  $I_L$ . Here to find  $V_m$  we compare the theoretical limit  $\eta_{FF}$  formulated by Green et al. (2003) and Shockley and Queisser (1961) given by **Eqs 14, 15**.

$$\eta_{FF,Green} = \frac{\frac{V_{OC}}{V_c} - \ln \ln \left( \frac{V_{OC}}{V_c} + 0.72 \right)}{\frac{V_{OC}}{V_c} + 1} \quad (14)$$

$$\eta_{FF,Shockley} = \frac{\left( \frac{V_m}{V_c} \right)^2}{\left( 1 + \frac{V_m}{V_c} - e^{-\frac{V_m}{V_c}} \right) \times \frac{V_{OC}}{V_c}} \quad (15)$$

where  $V_c$  is the thermal voltage given as follows:



$$V_c = \frac{kT_{cell}}{q} \tag{16}$$

To find  $V_m$ , Eqs 14, 15 and solve for unknown  $V_m$

### 3.4.4 Efficiency of the TPV System

The efficiency of the TPV system which includes back surface reflector and spectral filters with reflectivity R is given as follows (Scranton et al., 2016):

$$\eta = \frac{I_L \times V_m}{\int_0^\infty \frac{\epsilon \times C_1}{\lambda^5 [\exp(\frac{C_2}{\lambda T}) - 1]} d\lambda - \int_0^{\lambda_{filter}} \frac{\epsilon \times C_1}{\lambda^5 [\exp(\frac{C_2}{\lambda T}) - 1]} d\lambda - R \int_{\lambda_g}^\infty \frac{\epsilon \times C_1}{\lambda^5 [\exp(\frac{C_2}{\lambda T}) - 1]} d\lambda} \tag{17}$$

The aforementioned relation Eq. 17 shows how the efficiency of the system varies with the incorporation of photon recycling technologies. The output power of the cell remains the same but the effective energy at the input of the cell is decreased by the factor of the reflectivity of each spectral control technique incorporated. If only BSR is included in the system then the efficiency is enhanced to a certain extent, on the other hand, when filtering technology is incorporated along with the BSR (second term in the denominator), low energy photons are filtered, which further reduces the energy at the input by the factor of reflectivity R of the filter and hence the overall efficiency of the TPV system is enhanced. The efficiency of such hybrid TPV systems will always be greater than the systems which use single technology, that is, either spectral filter or BSR for photon recycling.

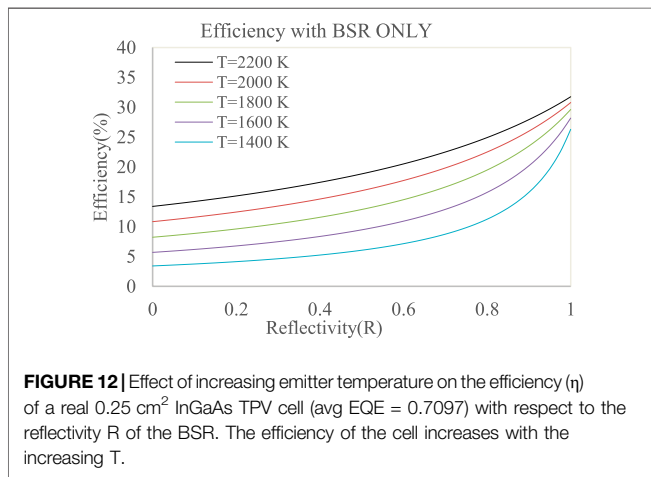
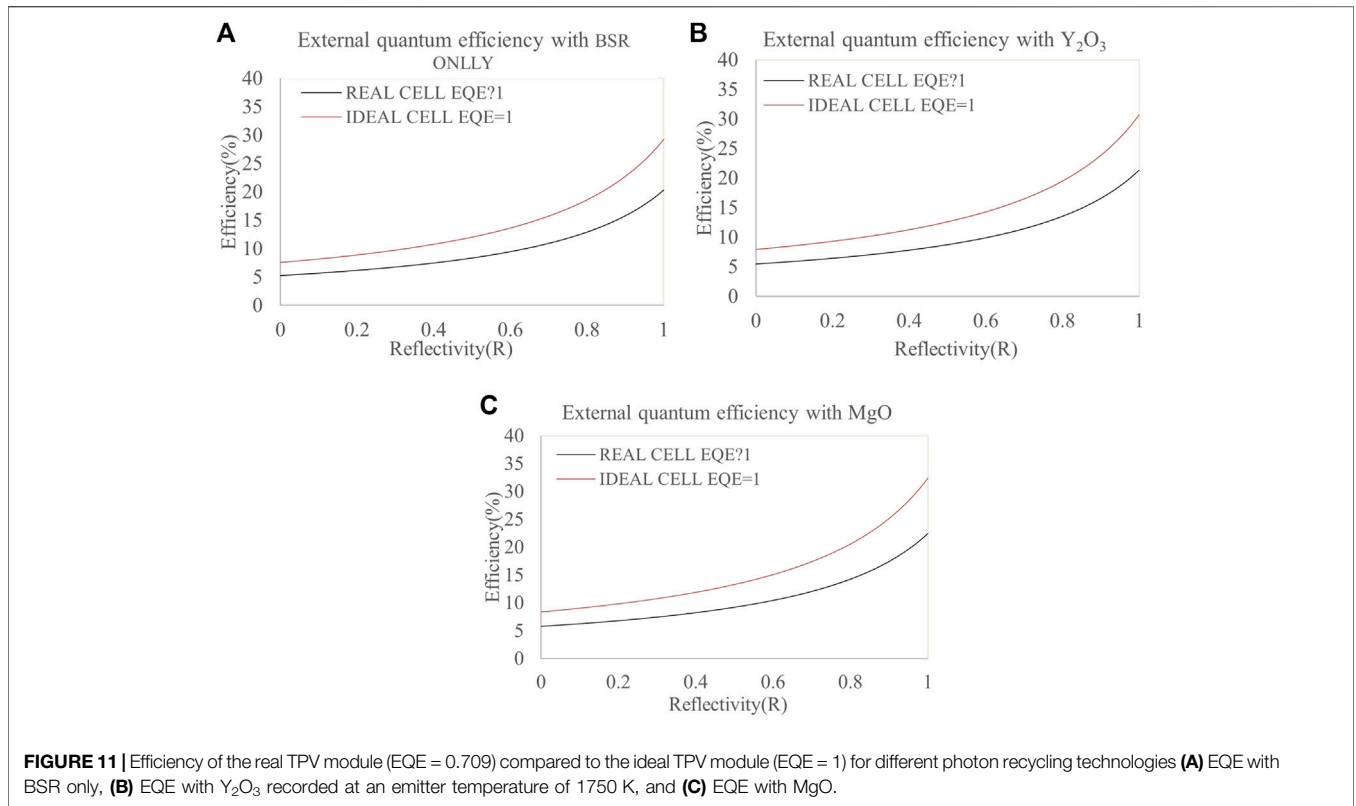
## 4 RESULTS AND DISCUSSION

### 4.1 Cell Selection Based on Spectral Emissive Power

Table 2 shows different PV cell materials along with their bandgap energy  $E_g$  and bandgap wavelength  $\lambda_g$  through Eq. 3. Through Wein’s displacement law in Eq. 2 the peak wavelength,  $\lambda_p$  has been calculated as  $1.656 \mu\text{m}$  at the emitter temperature of 1750 K. Lenert et al. (2014) has concluded that for the optimum TPV cell, the bandgap and the peak wavelengths should be well-

matched to minimize the thermalization losses and achieve better performances. Figure 8 compares the useful region of the emissive power above the bandgap for all the materials listed in Table 2 to the plank’s distribution curve for a TPV cell at a constant temperature. The analysis was performed for a single cell and not for the array that is why no mismatch losses are considered and the irradiance is taken as 100% (Kazim et al., 2020).

It can be noted from Figure 8 that the CGS and CdTe cells have the lowest bandgap wavelengths and hence the lowest spectral emissive power region above the bandgap ( $\eta_{E > E_g}$  is 0.377% and 1.01%). Si is the most widely used material in the world of photovoltaics (Saga, 2010) but as can be seen from Figure 8, its bandgap wavelength is very much smaller than the peak wavelength and the area of spectral power is not large enough as well ( $\eta_{E > E_g} = 5.83\%$ ). CIS behaves as the Si does. In the case of InGaAsSb ( $E_g = 0.55 \text{ eV}$ ), the bandgap energy is the least, which shows that an exceedingly small amount of energy is needed to generate the electron-hole pair. However, the bandgap wavelength is much higher than the peak wavelength ( $\lambda_g - \lambda_p = 0.6 \mu\text{m}$ ) and this higher bandgap wavelength results in overheating of the cell and thermalization losses (Kazim et al., 2020). Ge, GaSb, and InGaAs have less difference between the bandgap wavelength and Wein’s peak wavelength of the emitter, that is, 0.2, 0.07, and  $0.02 \mu\text{m}$ , respectively, and the percentage area above the bandgap are also within the acceptable range (34.44%, 28.17%, and 26.31% respectively). Furthermore, these materials which ( $E_g > 0.6 \text{ eV}$ ) need lesser control for Auger recombination and lower series resistances improve the TPV cell performance (Tuley and Nicholas, 2010). GaSb and InGaAs cells have the advantage over Ge (single element) cells in that their bandgaps can be tuned by changing the stoichiometry of these cells. For ternary and quaternary PV cells, as the number of materials increases, the spectral power and efficiency also increase with even lower emitter temperatures (Tong et al., 2015). InP substrates are the lower frequency substrates, they also help in overcoming the lower efficiency of TPV cells. Therefore, the



$In_{0.53}Ga_{0.47}As$  grown on the InP substrate, due to its widely available data reported in the literature and uses in TPV technology, are selected for further analysis (Seyf et al., 2016; Wang et al., 2020).

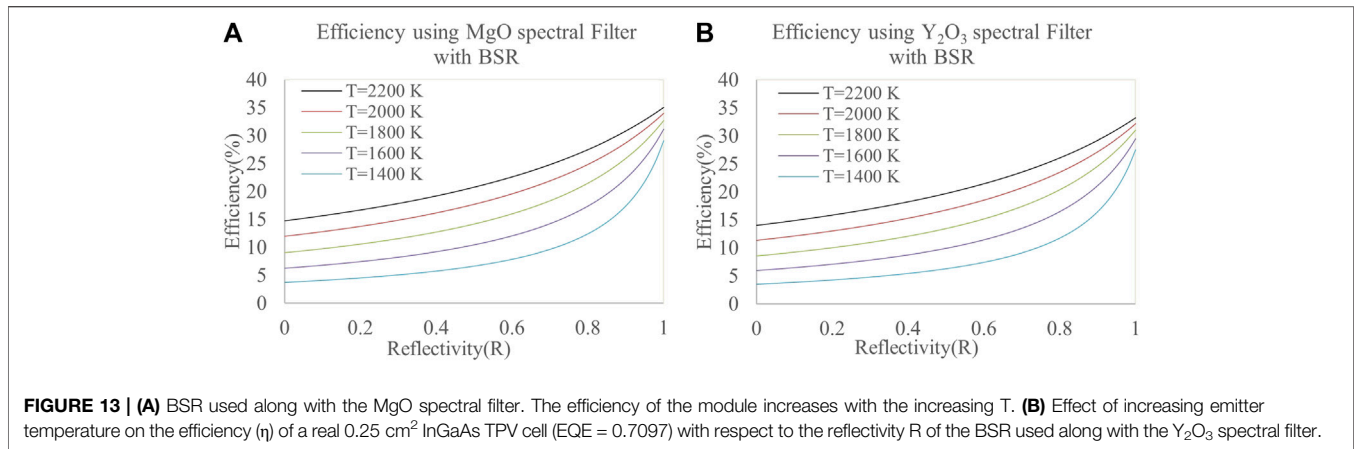
### 4.2 Selection of the Filter

The selected filter must have a wide transparency range and high melting point because of the high emitter temperatures. FSS and TCO filters are not used as they are very costly and have high absorption near the plasma frequency, respectively. All-dielectric

filters on the other hand show interference among different filter layers and have small wavelength ranges (Machrafi, 2012). Crystalline materials  $Y_2O_3$  and MgO are used for filtering the low bandgap photons from the emission spectra of the emitter since these have a wide transmission range ( $0.3 - 7\mu m$ ) and ( $0.4 - 7\mu m$ ), respectively. The photons with longer wavelengths are filtered and the interference at the cell surface is reduced which helps to maintain the temperature of the cell at 300 K as well. The selected materials also have high melting points which help them in sustaining the high amount of heat energy coming from the radiator source. As the efficiency of the cell is the function of temperature and since these filters also act as heat shields and do not allow the conduction of heat from the radiator body to the cell, the cell temperature does not increase (Machrafi, 2012).

### 4.3 Efficiency of the Real Cell

The  $In_{0.53}Ga_{0.47}As$  grown on the InP substrate, the region of the spectral emissive power that is above the bandgap of InGaAs ( $E_g = 0.74 \text{ eV}$ ) is the useful portion for the generation of electron-hole pairs and hence electrical power. For the emitter temperature of 1750 K, the useful emissive power region is as shown in Figure 9. For the real module (EQE  $\neq$  1) the average external quantum efficiency is calculated using Eq. 7 and found to be 0.7097 (Kazim et al., 2020). The photocurrent  $I_L$  for a  $0.25 \text{ cm}^2$  module is calculated using Eq. 11 and is 1.44 A which takes the total number of photons falling on the TPV cell into account. Photocurrent density  $I_{ph}$  is  $5.79 \text{ A/cm}^2$ . Eq. 12 gives values of the



dark saturation currents  $I_{01} = 3.22 \times 10^{-9} \text{ A}$  and  $I_{02} = 1.83 \times 10^{-5} \text{ A}$  that are found by putting  $R_s = 0.25 \text{ m}\Omega\text{cm}^2$  for an InGaAs cell (Tuley et al., 2012). These values of saturation currents are calculated using the data sets from **Figure 5**. Relations (13–16) are used to determine the values of  $V_{oc}$  and  $V_m$ , which are 0.51 and 0.43, V respectively. The effect of reflectivity (R) on the efficiency ( $\eta$ ) of the TPV cell is shown in **Figure 10**.

As can be seen from the graph in **Figure 10**, the efficiency of the TPV cell with absolutely no reflectivity ( $R = 0$ ) is exceptionally low, that is, 5.5%. But as the reflectivity is increased to almost 1, the efficiency of the cell at the emitter temperature of 1750 K also increases and reaches almost 20.3% for a real TPV cell.

## 4.4 Comparison of Efficiency Enhancement Achieved Through This Work Compared to the Previous Studies

### 4.4.1 The Efficiency of the Real Cell Vs. the Ideal Cell

It has been recorded that the external quantum efficiency can be improved using a cell material that has a high coefficient of absorption (Wang et al., 2020), high reflective coatings at the back of the cell (BSR), and using textured front surface (Ray et al., 2015), using cells with lower bandgap energy that are composed of quantum nanostructures (Datas et al., 2017) and the use of multijunction or tandem cells can also improve the EQE (Moss et al., 2018). In this section, the efficiency of the real TPV cell (EQE  $\neq 1$ ) is compared with the ideal one (EQE = 1) with different photon recycling technologies. For the EQE = 1, it is supposed that all the photons that fall on the surface of the TPV cell, are utilized by the cell, and produce electrical power through the external circuit by generating an equal number of electron-hole pairs (Kazim et al., 2020).

For an ideal TPV cell, the saturation currents  $I_{01}$  and  $I_{02}$  are the same as calculated for the real case scenario. The photocurrent and the photocurrent density are calculated as  $I_L = 2.04 \text{ A}$  and  $I_{ph} = 8.15 \text{ A/cm}^2$ , respectively.  $V_{oc}$  and  $V_m$  are 0.52 and 0.44 V, respectively. The efficiencies of the real and ideal TPV module with BSR, with  $\text{Y}_2\text{O}_3$  as a spectral filter and MgO as filter are compared in **Figure 11**, all recorded at the emitter temperature of

1750 K. **Figures 11A–C** show the existing room for improvement in a real TPV module. An ideal  $0.25 \text{ cm}^2$  InGaAs TPV cell (EQE = 1) can attain efficiencies for BSR,  $\text{Y}_2\text{O}_3$ , and MgO as high as 29.2%, 30.6%, and 32.3%, in contrast to 20.3%, 21.2%, and 22.4% efficiencies of the real TPV cell (EQE = 0.709), at the maximum reflectivity of 1 and an average temperature of 1750K, respectively. It can be seen that the real (EQE = 0.709) and the ideal (EQE = 1) TPV cell which uses MgO filters between the emitter and the cell, attain better efficiencies of 22.4% and 32.3%, respectively. Although compared to the earlier studies which used BSR behind the cell surface reported the efficiencies of 20.3% and 29.2% for the real (EQE = 0.709) and the ideal (EQE = 1) TPV cell, respectively, at 1750 K emitter temperature (Kazim et al., 2020).

### 4.4.2 Effect of Emitter Temperature on Efficiency

As the temperature of the blackbody emitter is increased, the spectral emissive power and hence the photon flux above the bandgap is also improved which increases the photogenerated current (Machrafi, 2012). Hence, the increasing emitter temperature improves the efficiency of the TPV cell. **Figure 12** shows the performance of the TPV cell with the use of BSR only as the emitter temperature is increased. The efficiency of the cell goes from 26.2% to 31.7% as the temperature is raised from 1400 to 2200 K. **Figures 13A,B** illustrate how the performance of the TPV cell is improved at elevated emitter temperatures as the spectral filters are incorporated along with the BSR with the increasing emitter's temperature. The efficiency of the TPV cell that uses  $\text{Y}_2\text{O}_3$  spectral filter with BSR at maximum reflectivity,  $R = 1$  (**Figure 13B**) improves efficiency from 27 to 33.2% as the temperature goes from 1400 to 2200 K. Similarly, with MgO as the spectral filter used along with BSR (**Figure 13A**), the efficiency of the cell is further improved from 29 to 35% as the temperature is increased. This increase in the efficiencies is since the low energy bandgap photons and hence the interference at the surface of the cell is reduced with the incorporation of the filter and cell temperature is also maintained at 303 K. Hence, the efficiency of the TPV system is enhanced as the temperature of the emitter is elevated. The previous studies have shown that this increase in efficiency reaches 31.7% at 2200 K emitter

**TABLE 3 |** Spectral technology-wise efficiency improvement; ( $\eta$  at the emitter temperatures of 1400, 1600, 1800, 2000, and 2200 K).

Temperature (K)	$\eta$ with only BSR (%)	$\eta$ with $Y_2O_3$ (%)	$\eta$ with MgO (%)
1400	26.3	27.5	29
1600	28.2	29.5	31.1
1800	29.6	31	32.6
2000	30.8	32.2	34
2200	31.7	33.2	35

temperature if only BSR is incorporated in the system (Kazim et al., 2020). However, if hybrid spectral optimization

technologies are used, that is, BSR paired with front spectral filters, the efficiencies can be improved even further.

### 4.4.3 Effect of Different Filtering Technologies on Efficiency

Spectral control technologies have proven to enhance the efficiencies of the current TPV systems. **Figures 14A–E** demonstrate how different photon recycling technologies including BSR, MgO, and  $Y_2O_3$  spectral filters, improve the overall efficiency of the cell at various emitter temperatures. The efficiency values at maximum reflectivity ( $R = 1$ ), from **Figures 14A–E** are extracted and listed in tabular form in **Table 3**. The crystalline spectral filters are better than the

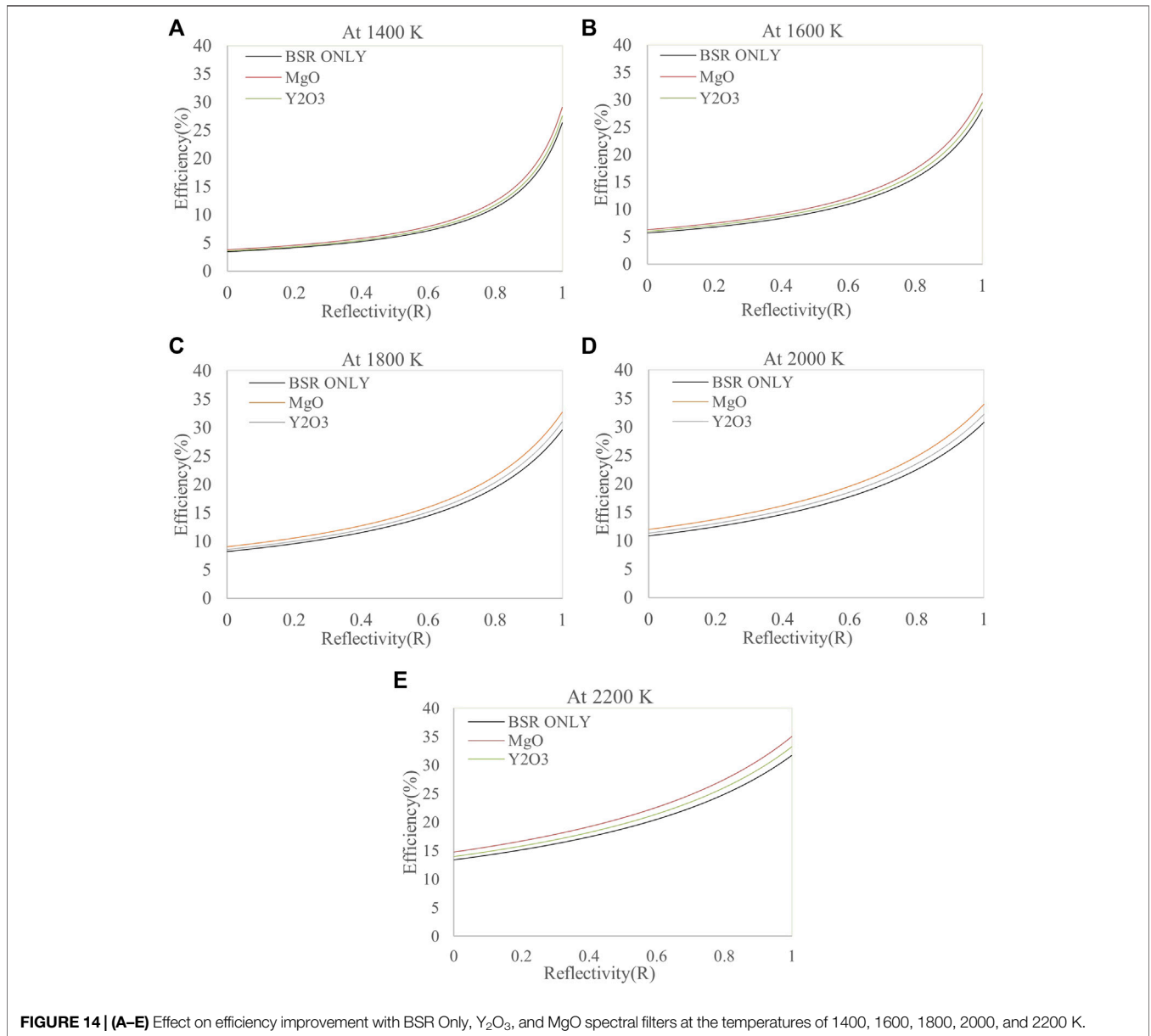


**FIGURE 14 | (A–E)** Effect on efficiency improvement with BSR Only,  $Y_2O_3$ , and MgO spectral filters at the temperatures of 1400, 1600, 1800, 2000, and 2200 K.

BSRs and they can increase the efficiency of the cell much more than BSRs. The MgO spectral filter maximizes the efficiency improvement rather than  $Y_2O_3$ . The overall efficiency with MgO is 35% which is more than with the use of BSRs only, that is, 31.7% (Kazim et al., 2020). With MgO as the front filter at 2200 K there is an almost 3.3% efficiency increase while with  $Y_2O_3$  as a filter, this increase is 1.4% more than the previous technique of BSR. This shows that there is quite a room for improvement in the efficiencies of the TPV systems with the incorporation of hybrid spectral controls.

## 5 CONCLUSION

In this work, the design parameters and configuration of front filters with BSRs are studied under 2500 K temperature of the emitter. It is found that cells with moderate bandgap energy like Ge (0.66 eV), GaSb (0.72 eV), and InGaAs (0.74 eV) are most favorable as their bandgap wavelength is well-matched with the peak wavelength calculated through Wein's law, in addition, they provide lower recombination rates and high photon flux above the bandgap region. It can be concluded that MgO is better than the  $Y_2O_3$  spectral filter because with the use of the MgO front filter at 2200 K there is about a 3.3% efficiency increase while with the  $Y_2O_3$  spectral filter used along with BSR, this increase is 1.4% than the previous technique of using BSR only. The overall

efficiency attained with the proposed hybrid technique, that is, the use of MgO as a filter along with BSR, is 35% and this hybrid technique also helps in reducing the interference at the cell surface and maintaining the cell temperature at almost 303 K while acting as a heat shield between the emitter and the cell. Thus, with such improvements in research, TPV has the capability to replace the CSP plant turbine.

## DATA AVAILABILITY STATEMENT

The raw data supporting the conclusion of this article will be made available by the authors, without undue reservation.

## AUTHOR CONTRIBUTIONS

MU, AK, and AS were involved in experimentation and the other authors helped in data analysis and write up.

## SUPPLEMENTARY MATERIAL

The Supplementary Material for this article can be found online at: <https://www.frontiersin.org/articles/10.3389/fenrg.2022.917419/full#supplementary-material>

## REFERENCES

- Anjani, N. R. (2021). *The Form of Jakarta-Berlin Paradiplomacy in Sister City Cooperation in the Field of Culture under International Relations*.
- Barber, J. (2018). Hydrogen Derived from Water as a Sustainable Solar Fuel: Learning from Biology. *Sustain. Energy Fuels* 2 (5), 927–935. doi:10.1039/c8se00002f
- Bernardi, M. P., Dupré, O., Blandre, E., Chapuis, P. O., Vaillon, R., and Francoeur, M. (2015). Impacts of Propagating, Frustrated and Surface Modes on Radiative, Electrical and Thermal Losses in Nanoscale-Gap Thermophotovoltaic Power Generators. *Sci. Rep.* 5 (1), 11626. doi:10.1038/srep11626
- Boriskina, S. V., Tong, J. K., Ferry, V., Michel, J., and Kildishev, A. (2015). Breaking the Limits of Optical Energy Conversion. *Opt. Photonics News* 26 (7), 48–51. doi:10.1364/opn.26.7.000048
- Boulkhrachef, S. (2019). Higher-Order Sliding Mode Control of a Wind Energy Conversion System. *Nonlinear Dyn. Syst. Theory* 19 (4), 486–496.
- Bouid, F., and Dehimi, L. (2012). Performance Evaluation of a GaSb Thermophotovoltaic Converter. *Rev. Des. Energies Renouvelables* 15 (3), 383–397.
- Breitenstein, O., Rißland, S., and cells, s. (2013). A Two-Diode Model Regarding the Distributed Series Resistance. *Sol. Energy Mater. Sol. Cells* 110, 77–86. doi:10.1016/j.solmat.2012.11.021
- Cabrera, A., Ramos, A., Artacho, I., Gomez, M., Gavin, K., Marti, A., et al. (2018). “Thermophotovoltaic Efficiency Measurement: Design and Analysis of a Novel Experimental Method,” in 2018 Spanish Conference on Electron Devices (CDE) (Salamanca, Spain: IEEE). doi:10.1109/cde.2018.8596820
- Cendula, P., Mayer, M. T., Luo, J., and Grätzel, M. (2019). Elucidation of Photovoltage Origin and Charge Transport in Cu<sub>2</sub>O Heterojunctions for Solar Energy Conversion. *Sustain. Energy Fuels* 3 (10), 2633–2641. doi:10.1039/c9se00385a
- Charache, G., DePoy, D. M., Baldasaro, P. F., and Campbell, B. C. (1996). Thermophotovoltaic Devices Utilizing a Back Surface Reflector for Spectral Control. *AIP Conf. Proc.* 358, 339. doi:10.1063/1.49697
- Chen, M., Chen, X., Yan, H., and Zhou, P. (2021). Theoretical Design of Nanoparticle-Based Spectrally Emitter for Thermophotovoltaic Applications. *Phys. E Low-Dimensional Syst. Nanostructures* 126, 114471. doi:10.1016/j.physe.2020.114471
- Chen, M., He, Y., Huang, J., and Zhu, J. (2016). Synthesis and Solar Photo-Thermal Conversion of Au, Ag, and Au-Ag Blended Plasmonic Nanoparticles. *Energy Convers. Manag.* 127, 293–300. doi:10.1016/j.enconman.2016.09.015
- Chen, M., He, Y., Ye, Q., Zhang, Z., and Hu, Y. (2019). Solar Thermal Conversion and Thermal Energy Storage of CuO/Paraffin Phase Change Composites. *Int. J. Heat Mass Transf.* 130, 1133–1140. doi:10.1016/j.ijheatmasstransfer.2018.11.026
- Chen, M., He, Y., Zhu, J., and Wen, D. (2016). Investigating the Collector Efficiency of Silver Nanofluids Based Direct Absorption Solar Collectors. *Appl. Energy* 181, 65–74. doi:10.1016/j.apenergy.2016.08.054
- Cherp, A., Vinichenko, V., Jewell, J., Suzuki, M., and Antal, M. (2017). Comparing Electricity Transitions: A Historical Analysis of Nuclear, Wind and Solar Power in Germany and Japan. *Energy Policy* 101, 612–628. doi:10.1016/j.enpol.2016.10.044
- Chirumamilla, M., Krishnamurthy, G. V., Knopp, K., Krekeler, T., Graf, M., J alas, D., et al. (2019). Metamaterial Emitter for Thermophotovoltaics Stable up to 1400 °C. *Sci. Rep.* 9 (1), 7241. doi:10.1038/s41598-019-43640-6
- Coutts, T. (1999). *Renewable Sustainable Energy Rev.*
- Coyle, E. D., and Simmons, R. A. (2014). *Understanding the Global Energy Crisis*. West Lafayette, Indiana, USA: Purdue University Press.
- Datas, A., and Cells, S. (2015). Optimum Semiconductor Bandgaps in Single Junction and Multijunction Thermophotovoltaic Converters. *Sol. Energy Mater. Sol. Cells* 134, 275–290. doi:10.1016/j.solmat.2014.11.049
- Datas, A., Martí, A., and Cells, S. (2017). Thermophotovoltaic Energy in Space Applications: Review and Future Potential. *Sol. Energy Mater. Sol. Cells* 161, 285–296. doi:10.1016/j.solmat.2016.12.007
- Datas, A., and Vaillon, R. (2021). “Thermophotovoltaic Energy Conversion,” in *Ultra-High Temperature Thermal Energy Storage, Transfer and Conversion* (Amsterdam, Netherlands: Elsevier), 285–308. doi:10.1016/b978-0-12-819955-8.00011-9
- Erdoğan, N., Mungan, A., and Bilensoy, E. (2010). Preparation and Characterization of Cationic Nanoparticles Loaded with Mitomycin C by

- Double Emulsion and Ionotropic Gelation Techniques. *J. Control Release* 148 (148), e78–9. doi:10.1016/j.jconrel.2010.07.015
- Ferrari, C., Melino, F., Pinelli, M., Spina, P. R., and Venturini, M. (2014). Overview and Status of Thermophotovoltaic Systems. *Energy Procedia* 45, 160–169. doi:10.1016/j.egypro.2014.01.018
- Goorha, P. (2010). “Modernization Theory,” in *The International Studies Encyclopedia*. Editor R. A. Denmark (Malden, Ma: Wiley-Blackwell).
- Green, M. A., Emery, K., King, D. L., Igari, S., and Warta, W. (2003). Solar Cell Efficiency Tables (Version 22). *Prog. Photovolt. Res. Appl.* 11, 347–352. doi:10.1002/pip.499
- Güney, T. (2019). Renewable Energy, Non-Renewable Energy and Sustainable Development. *Int. J. Sustain. Dev. World Ecol.* 26 (5), 389–397. doi:10.1080/13504509.2019.1595214
- Hank, C., Sternberg, A., Köppel, N., Holst, M., Smolinka, T., Schaadt, A., et al. (2020). Energy Efficiency and Economic Assessment of Imported Energy Carriers Based on Renewable Electricity. *Sustain. Energy Fuels* 4 (5), 2256–2273. doi:10.1039/d0se00067a
- Hansen, K., Breyer, C., and Lund, H. (2019). Status and Perspectives on 100% Renewable Energy Systems. *Energy* 175, 471–480. doi:10.1016/j.energy.2019.03.092
- Heidarzadeh, H., Rostami, A., and Dolatyari, M. (2020). Management of Losses (Thermalization-Transmission) in the Si-QDs Inside 3C-SiC to Design an Ultra-High-Efficiency Solar Cell. *Mater. Sci. Semicond. Process.* 109, 104936. doi:10.1016/j.mssp.2020.104936
- Hejri, M., Mokhtari, H., Azizian, M. R., Ghandhari, M., and Soder, L. (2014). On the Parameter Extraction of a Five-Parameter Double-Diode Model of Photovoltaic Cells and Modules. *IEEE J. Photovoltaics* 4 (3), 915–923. doi:10.1109/jphotov.2014.2307161
- Henry, A., Prasher, R., and Science, E. (2014). The Prospect of High Temperature Solid State Energy Conversion to Reduce the Cost of Concentrated Solar Power. *Energy Environ. Sci.* 7 (6), 1819–1828. doi:10.1039/c4ee00288a
- Hristov, H. D. (2016). “Fresnel Zone Plate Antenna,” in *Handbook of Antenna Technologies* (Berlin, Germany: Springer), 1187–1248. doi:10.1007/978-981-4560-44-3\_42
- Huang, R. K., Wang, C. A., Connors, M. K., Turner, G. W., and Dashiell, M. (2004). Hybrid Back Surface Reflector GaInAsSb Thermophotovoltaic Devices. *AIP Conf. Proc.* 738, 329. doi:10.2172/836454
- Isobe, K., Okino, R., and Hanamura, K. (2020). Spectral Absorptance of a Metal-Semiconductor-Metal Thin-Multilayer Structured Thermophotovoltaic Cell. *Opt. Express* 28 (26), 40099–40111. doi:10.1364/oe.410828
- Jena, D., Ramana, V. V., and Reviews, S. E. (2015). Modeling of Photovoltaic System for Uniform and Non-Uniform Irradiance: A Critical Review. *Renew. Sustain. Energy Rev.* 52, 400–417. doi:10.1016/j.rser.2015.07.079
- Jung, K. W., Sohn, M. R., Lee, H. M., Yang, I. S., Sung, S. D., Kim, J., et al. (2018). Silver Bismuth Iodides in Various Compositions as Potential Pb-Free Light Absorbers for Hybrid Solar Cells. *Sustain. Energy Fuels* 2 (1), 294–302. doi:10.1039/c7se00477j
- Karalis, A., and Joannopoulos, J. D. (2017). Transparent and ‘opaque’ Conducting Electrodes for Ultra-Thin Highly-Efficient Near-Field Thermophotovoltaic Cells. *Sci. Rep.* 7 (1), 14046. doi:10.1038/s41598-017-13540-8
- Kazim, A. H., Asif, M., Nadeem, K., Shoukat, Z., Nazir, R., Malik, M. S., et al. (2020). Efficiency Enhancement of a Thermophotovoltaic System Integrated with a Back Surface Reflector. *IEEE Access* 8, 153226–153239. doi:10.1109/access.2020.3017504
- Khalid, A., Norello, R., N. Abraham, A., Tetienne, J.-P., J. Karle, T., W. C. Lui, E., et al. (2019). Biocompatible and Biodegradable Magnesium Oxide Nanoparticles with *In Vitro* Photostable Near-Infrared Emission: Short-Term Fluorescent Markers. *Nanomaterials* 9 (10), 1360. doi:10.3390/nano9101360
- Kim, J. M., Park, K. H., Kim, D. S., Hwang, B. Y., Kim, S. K., Chae, H. M., et al. (2018). Design and Fabrication of Spectrally Selective Emitter for Thermophotovoltaic System by Using Nano-Imprint Lithography. *Appl. Surf. Sci.* 429, 138–143. doi:10.1016/j.apsusc.2017.07.300
- Köstlin, H. (1982). Application of Thin Semiconductor and Metal Films in Energy Technology. *Adv. Solid State Phys.* 22, 229–254.
- Lee, E. (2018). *Synthesis and Luminescence Properties of Bi<sup>3+</sup>, Yb<sup>3+</sup> Co-Doped Y<sub>2</sub>O<sub>3</sub> Phosphor Powder and Thin Film for Application in Solar Cells*. Bloemfontein, SA: University of the Free State.
- Lenert, A., Bierman, D. M., Nam, Y., Chan, W. R., Celanović, I., Soljačić, M., et al. (2014). A Nanophotonic Solar Thermophotovoltaic Device. *Nat. Nanotech.* 9 (2), 126–130. doi:10.1038/nnano.2013.286
- Li, H., Yu, Y., Niu, F., Shafiq, M., and Chen, B. (2014). Performance of a Coupled Cooling System with Earth-To-Air Heat Exchanger and Solar Chimney. *Renew. Energy* 62, 468–477. doi:10.1016/j.renene.2013.08.008
- Machrafi, H. (2012). Philosophy for Controlling Auto-Ignition in an HCCI Engine. *Green Energy Technol.* 2012, 323–366. doi:10.2174/97816080528511201010323
- McClelland, A., and Mankin, M. (2018). *Optical Measurements for Scientists and Engineers: A Practical Guide*. Cambridge: Cambridge University Press.
- Meyer, E. L. (2017). Extraction of Saturation Current and Ideality Factor from Measuring Voc and Isc of Photovoltaic Modules. *Int. J. Photoenergy* 2017, 8479487. doi:10.1155/2017/8479487
- Midilli, A., Dincer, I., and Ay, M. (2006). Green Energy Strategies for Sustainable Development. *Energy Policy* 34 (18), 3623–3633. doi:10.1016/j.enpol.2005.08.003
- Moss, R. W., Henshall, P., Arya, F., Shire, G. S. F., Eames, P. C., and Hyde, T. (2018). Simulator Testing of Evacuated Flat Plate Solar Collectors for Industrial Heat and Building Integration. *Sol. Energy* 164, 109–118. doi:10.1016/j.solener.2018.02.004
- Nelson, R. E. (2003). TPV Systems and State-of-Art Development. *AIP Conf. Proc.* 653, 3. doi:10.1063/1.1539359
- Nicholas, R. J., and Tuley, R. S. (2012). Thermophotovoltaic (TPV) Devices: Introduction and Modelling. *Funct. Mater. Sustain. Energy Appl.* 2012, 67–90. doi:10.1533/9780857096371.1.67
- Norton, M., Amillo, A. M. G., and Galleano, R. (2015). Comparison of Solar Spectral Irradiance Measurements Using the Average Photon Energy Parameter. *Sol. Energy* 120, 337–344. doi:10.1016/j.solener.2015.06.023
- Onifade, S. T., Alola, A. A., Erdoğan, S., and Acet, H. (2021). Environmental Aspect of Energy Transition and Urbanization in the OPEC Member States. *Environ. Sci. Pollut. Res.* 28 (14), 17158–17169. doi:10.1007/s11356-020-12181-1
- Pethuraja, G. G., Welser, R. E., Sood, A. K., Lee, C., Alexander, N. J., Efstathiadis, H., et al. (2012). Effect of Ge Incorporation on Bandgap and Photosensitivity of Amorphous SiGe Thin Films. *Mater. Sci. Appl.* 3, 67. doi:10.4236/msa.2012.32010
- Pfister, N. A., and Vanderveelde, T. E. (2017). Selective Emitters for Thermophotovoltaic Applications. *Phys. Status Solidi A* 214 (1), 1600410. doi:10.1002/pssa.201600410
- Phan, H. T., Caney, N., Marty, P., Colasson, S., and Gavillet, J. (2009). Surface Wettability Control by Nanocoating: The Effects on Pool Boiling Heat Transfer and Nucleation Mechanism. *Int. J. Heat Mass Transf.* 52 (23–24), 5459–5471. doi:10.1016/j.ijheatmasstransfer.2009.06.032
- Rahmlow, T. D., Jr, DePoy, D. M., Fourspring, P. M., Ehsani, H., Lazo-Wasem, J. E., and Gratrix, E. J. (2007). Development of Front Surface, Spectral Control Filters with Greater Temperature Stability for Thermophotovoltaic Energy Conversion. *AIP Conf. Proc.* 890, 59. doi:10.1063/1.2711720
- Rahmlow, T. D., Jr, Lazo-Wasem, J. E., and Gratrix, E. J. (2004). “New Performance Levels for TPV Front Surface Filters,” in , 738, 180. *AIP Conf. Proc.* doi:10.1063/1.1841893
- Ray, M. K., Sasmal, S., and Maity, S. (2015). Improvement of Quantum Efficiency and Reflectance of GaAs Solar Cell. *Int. J. Eng. Res. General Sci.* 3 (2), 642.
- Riñland, S., and Breitenstein, O. (2013). Considering the Distributed Series Resistance in a Two-Diode Model. *Energy Procedia* 38, 167–175. doi:10.1016/j.egypro.2013.07.264
- Romero, M., Steinfeld, A., and Science, E. (2012). Concentrating Solar Thermal Power and Thermochemical Fuels. *Energy Environ. Sci.* 5 (11), 9234–9245. doi:10.1039/c2ee21275g
- Saga, T. (2010). Advances in Crystalline Silicon Solar Cell Technology for Industrial Mass Production. *NPG Asia Mater* 2, 96–102. doi:10.1038/asiamat.2010.82
- Sakakibara, R., Stelmakh, V., Chan, W. R., Ghebrehhan, M., Joannopoulos, J. D., Soljačić, M., et al. (2019). Practical Emitters for Thermophotovoltaics: A Review. *J. Photonics Energy* 9 (3), 032713. doi:10.1117/1.jpe.9.032713
- Sakr, E. S., Zhou, Z., and Bermel, P. (2014). High Efficiency Rare-Earth Emitter for Thermophotovoltaic Applications. *Appl. Phys. Lett.* 105 (11), 111107. doi:10.1063/1.4895932

- Scranton, G., Patrick Xiao, T., Ganapati, V., Holzrichter, J., Peterson, P. F., and Yablonoitch, E. (2016). "Highly Efficient Thermophotovoltaics Enabled by Photon Re-Use," in 2016 IEEE 43rd Photovoltaic Specialists Conference (PVSC) (Portland, OR, USA: IEEE). doi:10.1109/pvsc.2016.7749766
- Sergeev, A., and Waits, C. M. (2020). Effects of Photon Recycling, Trapping, and Reuse on Thermophotovoltaic Conversion Efficiency and Output Power. *J. Photonics Energy* 10 (3), 035501. doi:10.1117/1.jpe.10.035501
- Seyf, H. R., Henry, A., and Science, E. (2016). Thermophotovoltaics: A Potential Pathway to High Efficiency Concentrated Solar Power. *Energy Environ. Sci.* 9 (8), 2654–2665. doi:10.1039/c6ee01372d
- Shockley, W., and Queisser, H. J. (1961). Detailed Balance Limit of Efficiency of P-n Junction Solar Cells. *J. Appl. Phys.* 32 (3), 510–519. doi:10.1063/1.1736034
- Tong, J. K., Hsu, W. C., Huang, Y., Boriskina, S. V., and Chen, G. (2015). Thin-Film 'Thermal Well' Emitters and Absorbers for High-Efficiency Thermophotovoltaics. *Sci. Rep.* 5 (1), 10661. doi:10.1038/srep10661
- Tuley, R. S., and Nicholas, R. J. (2010). Band Gap Dependent Thermophotovoltaic Device Performance Using the InGaAs and InGaAsP Material System. *J. Appl. Phys.* 108 (8), 084516. doi:10.1063/1.3488903
- Tuley, R. S., Orr, J. M. S., Nicholas, R. J., Rogers, D. C., Cannard, P. J., and Dosanjh, S. (2012). Lattice-Matched InGaAs on InP Thermophotovoltaic Cells. *Semicond. Sci. Technol.* 28 (1), 015013. doi:10.1088/0268-1242/28/1/015013
- Utlu, Z. (2020). Thermophotovoltaic Applications in Waste Heat Recovery Systems: Example of GaSb Cell. *Int. J. Low-Carbon Technol.* 15 (2), 277–286. doi:10.1093/ijlct/ctz049
- Wang, C., Murphy, P. G., O'Brien, P. W., Shiau, D. A., Anderson, A. C., Liao, Z. L., et al. (2003). Wafer-Bonded Internal Back-Surface Reflectors for Enhanced TPV Performance. *AIP Conf. Proc.* 653, 473. doi:10.1063/1.1539402
- Wang, H., Ye, H., and Zhang, Y. (2014). Preparation and Performance Evaluation of Er<sub>2</sub>O<sub>3</sub> Coating-Type Selective Emitter. *Sci. China Technol. Sci.* 57 (2), 332–338. doi:10.1007/s11431-014-5456-x
- Wang, J., Zhang, J., Zhou, Y., Liu, H., Xue, Q., Li, X., et al. (2020). Highly Efficient All-Inorganic Perovskite Solar Cells with Suppressed Non-Radiative Recombination by a Lewis Base. *Nat. Commun.* 11 (1), 177–179. doi:10.1038/s41467-019-13909-5
- Warren, E. L., Deceglie, M. G., Rienäcker, M., Peibst, R., Tamboli, A. C., and Stradins, P. (2018). Maximizing Tandem Solar Cell Power Extraction Using a Three-Terminal Design. *Sustain. Energy Fuels* 2 (6), 1141–1147. doi:10.1039/c8se00133b
- Wernsman, B., Siergiej, R. R., Link, S. D., Mahorter, R. G., Palmisiano, M. N., Wehrer, R. J., et al. (2004). Greater Than 20% Radiant Heat Conversion Efficiency of a Thermophotovoltaic Radiator/Module System Using Reflective Spectral Control. *IEEE Trans. Electron Devices* 51 (3), 512–515. doi:10.1109/TED.2003.823247
- Tuley, R., Orr, J., Nicholas, R., Rogers, D., Cannard, P., and Dosanjh, S. (2012). "Lattice-Matched InGaAs on InP Thermophotovoltaic Cells," *Semiconductor Science and Technology*, 28(1), p. 015013.
- Yu, L., and Zunger, A. (2012). Identification of Potential Photovoltaic Absorbers Based on First-Principles Spectroscopic Screening of Materials. *Phys. Rev. Lett.* 108 (6), 068701. doi:10.1103/PhysRevLett.108.068701
- Yuan, X., Tavakkoli, F., and Vafai, K. (2015). Analysis of Natural Convection in Horizontal Concentric Annuli of Varying Inner Shape. *Numer. Heat. Transf. Part A Appl.* 68 (11), 1155–1174. doi:10.1080/10407782.2015.1032016
- Yuksel, A., Heltzel, A., and Howell, J. R. (2015). Design and Optimization of Thermal Selective Emitters for High-Efficiency Thermophotovoltaic (TPV) Power Generation. *Energy Sustain.* doi:10.1115/es2015-49581
- Zhou, Z., Sakr, E., Sun, Y., and Bermel, P. (2016). Solar Thermophotovoltaics: Reshaping the Solar Spectrum. *J. Nanophot.* 5 (1), 1–21. doi:10.1515/nanoph-2016-0011
- Zhou, Z., Yehia, O., and Bermel, P. (2016). Integrated Photonic Crystal Selective Emitter for Thermophotovoltaics. *J. Nanophot.* 10 (1), 016014. doi:10.1117/1.jnp.10.016014

**Conflict of Interest:** The authors declare that the research was conducted in the absence of any commercial or financial relationships that could be construed as a potential conflict of interest.

**Publisher's Note:** All claims expressed in this article are solely those of the authors and do not necessarily represent those of their affiliated organizations, or those of the publisher, the editors, and the reviewers. Any product that may be evaluated in this article, or claim that may be made by its manufacturer, is not guaranteed or endorsed by the publisher.

Copyright © 2022 Usman, Kazim, Shabbir, Abbasi and Sarwar. This is an open-access article distributed under the terms of the Creative Commons Attribution License (CC BY). The use, distribution or reproduction in other forums is permitted, provided the original author(s) and the copyright owner(s) are credited and that the original publication in this journal is cited, in accordance with accepted academic practice. No use, distribution or reproduction is permitted which does not comply with these terms.

## NOMENCLATURE

### Symbols

- C** Speed of light [ $\text{ms}^{-1}$ ]  
 **$C_1$**   $3.742 \times 108$  [ $\text{W}/\text{m}\mu\text{m}^{-4}$ ]  
 **$C_2$**   $1.4388 \times 104$  [ $\text{K}\mu\text{m}$ ]  
**E** Spectral emissive power [ $\text{W}/\text{m}^2$ ]  
**e** Exponential constant [2.71828]  
 **$E_b$  ( $0 \rightarrow \infty$ )** Blackbody spectral emissive power [ $\text{W}/\text{m}^2$ ]  
 **$E_g$**  Bandgap energy [eV]  
**H** Planck's constant [ $\text{m}^2/\text{kgs}$ ]  
 **$I_{01}$**  Ideal dark saturation current [A]  
 **$I_{02}$**  Non-ideal dark saturation current [A]  
 **$I_L$**  Photocurrent [A]  
 **$I_{ph}$**  Photocurrent density [ $\text{A}/\text{cm}^2$ ]  
 **$n_1$**  First diode ideality factor  
 **$n_2$**  Second diode ideality factor  
**Q** Electron charge [ $1.6 \times 10^{-19}\text{C}$ ]  
**R** BSR reflectivity  
 **$R_s$**  Series resistance [ohm]  
 **$R_{sh}$**  Shunt resistance [ohm]  
**T** Temperature of the emitter [K]  
 **$T_c$**  Temperature of the TPV cell [K]  
 **$V_c$**  Thermal voltage  
 **$V_m$**  Maximum voltage [A]  
 **$V_{oc}$**  Open-circuit voltage [V]

### Greek Symbols

- $\sigma$**  Stefan-Boltzmann constant [ $\text{W}/\text{m}^2\text{K}^4$ ]  
 **$\epsilon$**  Emissivity constant  
 **$\lambda$**  Wavelength [ $\mu\text{m}$ ]  
 **$\phi$**  Photon flux [ $\text{W}/\text{m}^2$ ]

**$\eta_{E > E_g}$**  Percentage of photons with energy above bandgap energy of the TPV cell [%]

**H** TPV conversion efficiency [%]

### Subscript and Superscript

- C** Cell  
**S** Series  
 **$S_h$**  Shunt  
**G** Bandgap  
 **$O_c$**  Open circuit  
 **$S_c$**  Short circuit  
**Ph** Photogenerated  
**M** Maximum

### Abbreviations

- BSR** Back surface reflector  
**CdTe** Cadmium telluride  
**CSP** Concentrated solar power  
**EQE** External quantum efficiency  
**FF** Fill factor  
**GaAs** Gallium arsenide  
**GaSb** Gallium antimonide  
**Ge** Germanium  
**InGaAs** Indium gallium arsenide  
**InGaAsSb** Indium gallium arsenide antimonide  
**InP** Indium phosphide  
**PV** Photovoltaic  
**Si** Silicon  
**SiGe** Silicon-germanium  
**TES** Thermal energy storage  
**TPV** Thermophotovoltaic